Experimental study on a new type of FBG-3D printed geogrid in embankment reinforcement

Mengxi Zhang[1*], *Hao Zhu*[1]

[1]Department of Civil Engineering, Shanghai University, Shanghai, 200072, China

Abstract. Fiber Bragg Grating (FBG) has been widely used in many civil engineering applications to sense strains and deformations. Combining the advantages of geosynthetics and FBG, this paper creatively presents a new type of FBG-3D printed geogrid, which allows reinforcement and accurate deformation monitoring. Geogrid is directly used as the packaging structure of FBG sensor, and the complete coordinated deformation between the grating monitoring areas of FBG sensor and geogrid is obtained through calibration test. A series of model tests were carried out with FBG-3D printed geogrid to study the influence of reinforcement layers and reinforcement spacing on the bearing capacity and deformation of embankment under cyclic loading. The test results showed that geogrid effectively improved the footing settlement, slope displacement of reinforced embankment under cyclic load, and the effect was more obvious with the decrease of geogrid spacing. The strain data inside the embankment was accurately collected by FBG sensors. Relevant research provides valuable suggestions for the development and application of new geosynthetics.

1 Introduction

With the passage of time, civil engineering infrastructures are subjected to many different external adverse effects and recession, which damages its structural integrity, causes serious security crisis and important economic losses. Therefore, it is essential to properly monitor and maintain these infrastructures to optimize their use and avoid potential risks.

In recent years, the emergence of new sensing technologies such as optical fiber sensors provides a broad prospect for structural monitoring [1-2]. Among them, discrete or quasi-distributed fiber Bragg grating sensor (FBG) has attracted much attention with advantages of small size, high precision, corrosion resistance, flexibility and electromagnetic interference resistance [3]. For example, Almubaied et al. [4] proposed an installation method of FBG sensors to monitor the corrosion of steel bars in concrete structures. You et al. [5] proposed a soil strain measurement method based on FBG sensing technology and successfully obtained real-time soil strain data. Yoshida et al. [6] used FBG arrays to conduct tests and developed a slope deformation monitoring system, which is helpful to provide key data support for structural safety analysis. It is worth noting that in practical use, the application of FBGs in its bare form is helpful to better transfer strain from the substrate. However,

* Corresponding author: mxzhang@i.shu.edu.cn

because these sensors are made of glass, their fatigue performance is poor and they are easy to be damaged, which is inconvenient to handle [7]. Therefore, FBG sensors are often protected in embedded applications.

In the traditional way, FBG sensors are usually tied to the component, which is easy to cause strain transfer loss [8]. This study, embeds FBG sensors into geogrid by 3D printing technology. In this way, geogrid, as a packaging structure, can not only protect FBG, but also self-sense the strain accurately. Then a series of model tests are carried out to verify the reliability of FBG sensor under cyclic load. The conclusions drawn from this study provide a basis for the development and expansion of new geosynthetic materials.

2 Materials and methods

2.1 Soil

Sand was used in this study as embankment backfill materials, with uniformity coefficient (Cu) of 2.74 and curvature coefficient (Cc) of 1.16. Figure 1 shows the particle size distribution curve of the sand, which is classified as poorly graded sand (SP) according with ASTM D2487. Through triaxial tests under different confining pressures, the internal friction angle of the sand was 35.2° at a relative density of 70%.

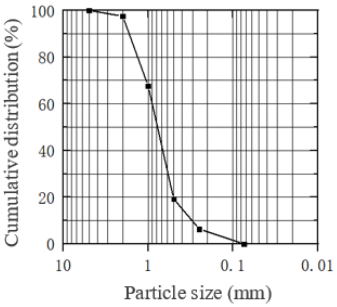

Fig. 1. Particle size distribution of the sand.

2.2 FBG sensor

FBG sensor is a monitoring element based on the sensitivity of optical equipment to light, and the grating is written into a specific area of fiber core by ultraviolet exposure. The working principle is shown in Figure 2. When the incident light is transmitted to the grating area through the optical fiber, the grating will only reflect the light signal centered at a specific wavelength (λ_B), and the wavelength determination formula can be expressed as Eq. (1):

$$\lambda_B = 2n_{eff}\Lambda \quad (1)$$

where n_{eff} is the effective refractive index of the fiber core and Λ is the grating period.

On the other hand, strain and temperature change the Bragg wavelength λ_B through the periodic expansion or contraction of the grating. The corresponding wavelength shift $\Delta\lambda_B$ can be obtained as Eq. (2):

$$\frac{\Delta\lambda_B}{\lambda_B} = K_\varepsilon\varepsilon + K_T\Delta T \quad (2)$$

where ε is the axial strain of grating, ΔT is the temperature change of grating, and K_T and K_ε are the sensitivity coefficients of strain and temperature, respectively.

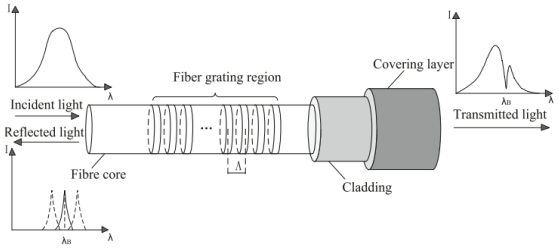

Fig. 2. Working principle of FBG sensors [9].

2.3 FBG-3D printed geogrid

Due to the particularity of optical fiber, it needs to be packaged and compatible with the tested element. In this experiment, the geogrid was directly used as the packaging structure of FBG sensor by 3D printing, and the deformation between the grating monitoring area and the geogrid was completely coordinated. Before 3D printing, the calibration experiment was carried out to determine the mathematical relationship between deformation and center wavelength. After 3D printing, the optical fiber outside the geogrid was protected by a PVC sleeve with a diameter of 2 mm and connected to the FBG demodulator. Table 1 describes the physical and mechanical properties of the FBG-3D printed geogrid.

Table 1. Properties of FBG-3D printed geogrid.

Parameter	Value
Aperture size (mm × mm)	10×10
Thickness (mm)	1.4
Tensile strength at 2% strain (kN/m)	3.5
Tensile modulus at 2% strain (kN/m)	175
Ultimate tensile strength (kN/m)	9.8

2.4 Test program

In this research, the model test was designed based on an embankment with a width of 8.8 m, a height of 4.4 m, and the slope ratio was 1:1.5. The relevant model size and scaling law referred to the previous method researched by Chen at al. [10]. Considering the axial symmetry, only 1/2 of the embankment was tested, and the scaling law was applied on the embankment with a scale of 1:20. Before sample preparation, Low friction silicone grease was used to minimize possible friction between the walls of the test box and the assembled soils. Then, 80 mm thick fill was laid at the bottom of the model box as embankment foundation. The model was established by static compaction of sand layer by layer. In this process, each layer was compacted to a relative density of 0.8. At the same time, the displacement sensors and FBG-3D printed geogrid were laid at the preset place, as shown in Figure 3. Table 2 shows the corresponding test conditions, including five groups of tests, which were carried out independently.

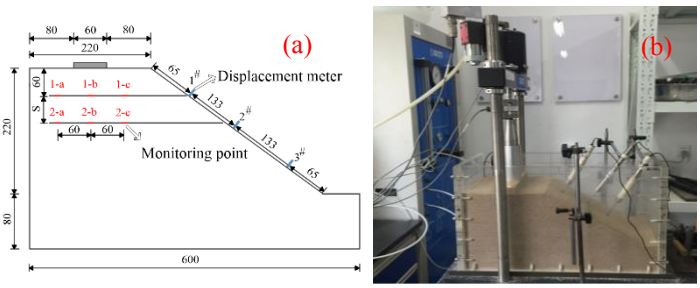

Fig. 3. A schematic view of the embankment model. (a) Model size of the embankment model (dimensions in mm). (b) Schematic diagram of the embankment model.

Table 2. Different test conditions of model test.

Test conditions	Reinforcement layer N	Depth of the first geogrid (mm)	Spacing (mm)
1	0	0	0
2	1	60	0
3	2	60	50
4	2	60	70
5	2	60	90

The load was applied through the loading plate. During the loading process, the test stopped when the displacement suddenly changed and the embankment suffered overall shear failure. In the cyclic loading test, 70% of the ultimate bearing capacity of unreinforced embankment under static loading, i.e. 20.3 kPa, was taken as the loading amplitude of cyclic loading, and the frequency was 1Hz. Figure 4 shows the loading waveform with a half sine shape in each cycle.

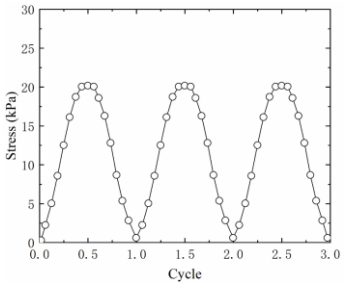

Fig. 4. Waveform of cyclic load.

3 Results and Discussion

3.1 Calibration test

In order to obtain the relationship between deformation and central wavelength of FBG, a calibration test was carried out. One side of the optical fiber was naturally drooped until the wavelength data remained stable. Then, a 20g weight was loaded on the optical fiber coil every 15s for 4 times. After loading, the weights were removed one by one in the same way. Figure 5 shows the test results, under the action of constant force, the wavelength of FBG is unchanged. But the wavelength of FBG is very sensitive to the changes in the force. The strain can be obtained by the action of force, which can be expressed as Eq. (3):

$$\varepsilon = F/EA \tag{3}$$

where F is the force on the optical fiber, E is the elastic modulus of the optical fiber, which is 62.5 GPa, and A is the cross-sectional area of the optical fiber, which is 8.767×10^{-8} m^2.

A corresponding relationship can be obtained by fitting the variation of wavelength and strain data under different forces, as shown in Eq. (4):

$$\varepsilon = 21.228\,\Delta\lambda/\lambda - 0.00003 \quad (4)$$

where ε is the strain of FBG, $\Delta\lambda$ is the amount of change in wavelength, λ is the value of wavelength. The coefficient of determination R^2 for this relationship is about 0.98, which shows a very good fit. This show that the FBG sensors embedded in 3D printed geogrid have good performance.

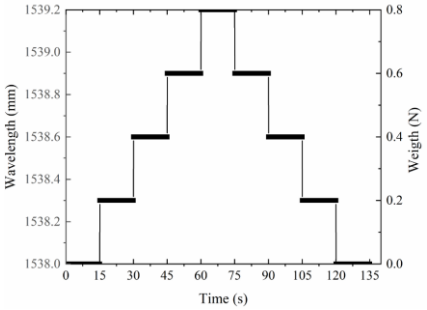

Fig. 5. Variation of FBG wavelength with weight and time.

3.2 Accumulative settlement

In order to obtain the vertical settlement law of the embankment after multiple cycles, cyclic load tests were carried out under different test conditions, and the results are shown in figure 6. It can be seen that when the number of cycles reaches 15,000, the cumulative settlement of the unreinforced embankment reaches 16.5 mm, resulting in a large deformation. But this situation is significantly improved with the reinforcement of geogrid. For the test condition of single-layer geogrid reinforcement, the cumulative settlement is reduced to 13.1mm, which is 20.6% lower than that without reinforcement. And the reinforcement effect increases with the increase of geogrid reinforcement layer. By controlling the spacing between the geogrids, the vertical settlements of the embankment under test condition 3, 4 and 5 are 9.9 mm (S=50 mm), 10.8 mm (S=70 mm) and 11.9 mm (S=90 mm), respectively, which are 40.1%, 34.5% and 27.9% lower than those without reinforcement. This shows that under the cyclic load, the sliding and rolling between sand particles increase the interlocking between geogrid and sand to produce a more stable soil structure, thus improving the deformation of the embankment. This remarkable reinforcement effect is more prominent after reducing the spacing of geogrids.

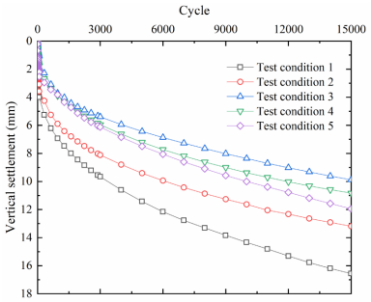

Fig. 6. Variations of the vertical settlement with number of cycles for embankment under different test conditions.

3.3 Slope displacement

Figure 7 shows the lateral dispalcement of the slope under cyclic loading. Because of the layout of geogrids, the lateral displacement of different positions of slope are quite different, mainly reflected in the upper part of the slope, and geogrid reinforcement has improved the deformation. At the same measuring point (No. 1#), the deformation of the unreinforced embankment is 6.22 mm, but that of the embankment reinforced with single layer of geogrid is 2.63 mm, which is reduced by 57.7%, showing a good ability to restrain soil deformation. This is because the interfacial friction effect between the soil and the geogrid can effectively restrain the lateral deformation of the soil, which makes it difficult for the soil on the upper part to produce large displacement. It is also noted that in the case of double-layer reinforcement, reducing the spacing between geogrids improves the limiting effect of geogrids on slope deformation, which is consistent with the law of cumulative settlement mentioned above.

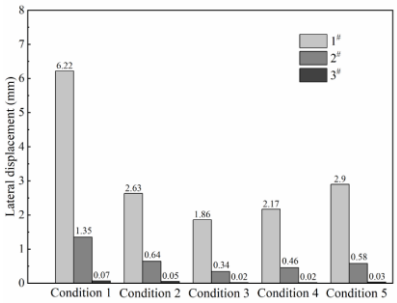

Fig. 7. Slope displacement of the embankment under different test conditions.

3.4 Deformation

It is generally difficult to accurately obtain the deformation data during the whole cyclic loading process. However, FBG sensor combined with geogrid through 3D printing technology can both have reinforcement and deformation monitoring. Figure 8 (a) shows the wavelength variation curve of measurement point 1-b under test condition 2, where the wavelength demodulator records the wavelength every 200 ms. In this process, the wavelength presents a trend of reciprocating growth. This is consistent with the cyclic load, which also reflects the reliability of FBG sensor measurement data. According to the formula in Section 3.1, the measured wavelength can be converted into strain data, and the data of each measuring point in test condition 3 with the best reinforcement effect is selected for analysis, as shown in figure 8 (b). The test results show that with the increase of number of cycles, the strain continues to increase. The position 1-b closest to the loading position in the horizontal direction has the largest strain and exceeds 2300 με after 15000 cycles. In the vertical direction, the strain data measured by FBG-3D printed geogrid decreases with the increase of layout depth. These strain data can provide necessary data to support the daily maintenance and monitoring of the road, and also have value for research and application.

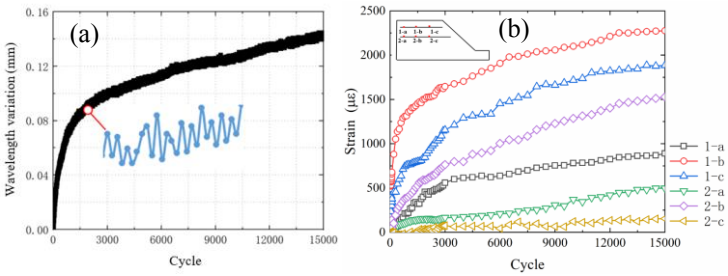

Fig. 8. Wavelength variation of FBG measuring point under different test conditions. (a) 1-b under test condition 2. (b) test condition 3.

4 Conclusions

In this paper, a FBG-3D printed geogrid that can monitor strain in real time was developed and applied to the model test of embankment. By controlling the number of geogrid layers and geogrid spacing, the deformation characteristics and mechanical properties of the embankment under cyclic load were studied. The conclusions of this research can be summarized as the following:

(1) The self-sensing geogrid designed by combining FBG sensor and 3D printing technology realizes the complete coordinated deformation between FBG sensor and geogrid. Through calibration experiment, the wavelength measured by FBG is effectively related to the strain of geogrid.

(2) Geogrid reinforcement effectively improves the vertical settlement and slope displacement of the embankment under cyclic load, and the reinforcement effect increases with the decrease of geogrid spacing.

(3) The position closest to the loading position in the horizontal direction has the largest strain. In the vertical direction, the strain data measured by FBG-3D printed geogrid decreases with the increase of layout depth.

References

1. A. Sounthararajah, L. Wong, N. Nguyen, H.H. Bui, J. Kodikara, Constr. Build. Mater. **156** (2017)
2. H. Zhao, D. Wu, M. Zeng, J. Ling, Transport. A: Trans. Sci. **15**, 1 (2019)
3. H.N. Li, D.S. Li, G.B. Song, Eng. Struct. **26**, 11 (2004)
4. O. Almubaied, H.K. Chai, M.R. Islam, K.S. Lim, C.G. Tan, IEEE Trans. Instrum. Meas. **66**, 8 (2017)
5. R.Z. You, L. Ren, G.B. Song, Measurement **139** 85-91 (2019)
6. Y. Yoshida, Y. Kashiwai, *Development of the monitoring system for slope deformations with fiber Bragg grating arrays*, In: Proceedings of SPIE, 296-303 (2002)
7. V. Ramani, K.S.C. Kuang, Construct. Build. Mater. **276**, 122129 (2021)
8. C.Y. Hong, Q. Yang, X.H. Sun, W.B. Chen, K.H. Han, Geotext. Geomembranes **49**, 6 (2021)
9. M.X. Zhang, H. Zhu, J. Yang, C.C. Q, A.A. Javadi, Geotext. Geomembranes **51**, 5 (2023)
10. J.F. Chen, X.P. Guo, R. Sun, S. Rajesh, S. Jiang, J.F. Xue, Geotext. Geomembranes **49**, 2 (2021)